Finding stable multi-component materials by combining cluster expansion with crystal structure predictions

Adam Carlsson (adam.carlsson@liu.se)
Linköpings University
Johanna Rosen
Linköping University
Martin Dahlqvist
Linköping University https://orcid.org/0000-0001-5036-2833

Article

Keywords:

Posted Date: June 16th, 2022

DOI: https://doi.org/10.21203/rs.3.rs-1673174/v1

Finding stable multi-component materials by combining cluster expansion and crystal structure predictions

Adam Carlsson*, Johanna Rosen, Martin Dahlqvist*

Materials Design, Department of Physics, Chemistry and Biology (IFM),
Linköping University, SE-581 83 Linköping, Sweden

Corresponding authors: adam.carlsson@liu.se, martin.dahlqvist@liu.se

Abstract

A desired prerequisite when performing a quantum mechanical calculation is to have an initial idea of the atomic positions within an approximate crystal structure. The atomic positions combined should result in a system located in, or close to, an energy minimum. However, designing low-energy structures may be challenging when prior knowledge is scarce, specifically for large multi-component systems where the degrees of freedom are close to infinite. In this paper we propose a method for identification of low-energy crystal structures in multi-component systems by combining cluster expansion and crystal structure prediction with density functional theory calculations. More importantly, we show that employing seed structures retrieved from cluster expansion models may significantly reduce the number of generations needed within the computationally demanding crystal structure prediction methodology. With this combined approach, we correctly identified the recently discovered $Mo_{4/3}Sc_{2/3}AlB_2$ *i*-MAB phase comprised of in-plane chemical ordering of Mo and Sc and with Al in a Kagomé lattice. This result demonstrates that a combined approach provides a path for identifying low-energy crystal structures in multi-component systems by employing the strengths from both the cluster expansion method and the crystal structure prediction framework. In addition, we also address examples when cluster expansion fails to account for important structural transformations in sublattices not part of the parametrization.

Introduction

Knowing the initial positions of atoms, or an approximate crystal structure prototype based on previous knowledge, is preferred when performing a quantum mechanical calculation. This is commonly not much of a problem for systems with one or two elemental components, e.g., unary, and binary systems, since these have been investigated thoroughly. Villers and Iwata estimates that all unary systems and 72 % of the potential binary systems have been experimentally studied [1]. However, for higher-order systems the potential elemental combinations increase rapidly, which is also reflected in the number of materials systems reported with only 16 % of ternary, 0.6 % of quaternary, and 0.03 % of quinary systems [1]. This demonstrates that experimental exploration of multi-component systems is still in its cradle and the avenues ahead are close to infinite. Theoretical studies may here serve as a complementary approach by predicting material combinations being most promising for future synthesis, as exemplified for ternary nitrides [2] and quaternary borides [3].

A certain group of materials which as of late have attracted a large interest are the atomically layered materials with interlayer interactions significantly stronger than van der Waals forces, hindering mechanical exfoliation. One such material group are the MAX phases [4] which are comprised of transition-metal carbide and nitride (MX) layers interleaved by an A-group elements. This structural arrangement along with the included elements often results in both metallic and ceramic properties [5]. Furthermore, selective etching, also known as chemical exfoliation, of the A-element from the MAX phases have spurred an increased interest and have emerged as an alternative route for the preparation of a two-dimensional (2D) family of materials known as MXenes [6, 7]. The search for additional multi-component materials with possibility for exfoliation is thus off great interest, and the discovery of in-plane chemically ordered MAX phase quaternaries, coined *i*-MAX [8-10], has enabled the synthesis of MXenes with in-plane chemical or vacancy ordering, such as $Mo_{4/3}Y_{2/3}C$, $Mo_{4/3}C$ and $W_{4/3}C$, showing promise for energy storage and catalysis [9-12].

Similar to MAX phases are layered metal boride-based materials, referred to as MAB phases, which consists of a transition metal (M), an A-group element (A) and boron (B). The mixing of metals in known ternary MAB phases have through theoretical guidance revealed both out-of-plane (*o*-MAB) and

in-plane (*i*-MAB) [3, 13] chemical ordering, where the latter phases have been converted into 2D derivatives coined boridene [14]. For the *o*-MAB phase, chemical ordering of metal atoms was achieved by taking advantage of two distinctly different crystallographic sites, and theoretical stability predictions revealed eleven stable *o*-MAB phases, out of which Ti_4MoSiB_2, of a tetragonal $I4/mcm$ symmetry, was synthesized. The *i*-MAB phases $Mo_{4/3}Y_{2/3}AlB_2$ and $Mo_{4/3}Sc_{2/3}AlB_2$ ($R\bar{3}m$ symmetry) were predicted by relaxing over 3,000 phases and were subsequently verified through powder synthesis [13]. The synthetized *i*-MAB phase $Mo_{4/3}Sc_{2/3}AlB_2$ with $R\bar{3}m$ symmetry will from this point forward be referred to as $Mo_{4/3}Sc_{2/3}AlB_2$, with fractional notations, whereas predicted phases of similar compositions will be referred to as $Mo_4Sc_2Al_3B_6$, with integer notations.

Different theoretical frameworks are utilized in the search for new low-energy crystal structures. Examples of such are crystal structure prediction (CSP) frameworks [15-17] and cluster expansion (CE) methods [18]. CSP methods are independent of any *a priori* information of the crystal structure and, in the case of the CSP code USPEX, uses evolutionary algorithms to search the chemical space for low-energy and possibly stable candidate compounds. For example Rybkovskiy *et al.,* studied the Mo-B system and predicted a new stable phase, MoB_5 [19], and Xu *et al.,* found a new stable binary multi-layered MnB_2 phase with properties resembling a hard multifunctional material [20]. In CSP searches of the W-Cr-B ternary system, W_4CrB_3 and W_2CrB_2 was found stable, in line with experiment, along with yet to be synthesized $WCrB_2$, WCrB, and WCr_2B [21]. Wang *et al.* predicted and synthesized the first hexagonal MAB phase Ti_2InB_2 [22] using the CSP. The latter discovery increased the field of synthesizable MAB phases from orthorhombic symmetries to also include hexagonal ones [13]. However, the computational demands increase drastically with increased complexity of the investigated system [23-25]. For example, Naumova *et al.* used CSP to search for structures in the quaternary C-H-N-O system under pressure, which required approximately 1,800,000 DFT relaxations [26].

An alternative to the computationally demanding CSP is the use of methods such as CE which, in contrast to CSP, requires an *a priori* defined crystal structure. The expansion is carried out on one or multiple sublattices where parameterization is used to express the configurational dependence of physical properties such as energy [27], band gap [28, 29] and magnetic interactions [30]. CE have also

been used to explore the configurational space in layered hexagonal MAX phases upon mixing of metals in 41 quaternary systems [31] where the alloys were classified into three regimes - phase separation, weak ordering, and strong ordering. It was found that $(V_{2/3}Zr_{1/3})_2AlC$ should phase segregate into V_2AlC and Zr_2AlC [31]. This result, however, contradicts the experimental discovery of the in-plane ordered $(V_{2/3}Zr_{1/3})_2AlC$ *i*-MAX phase [8]. The reason for this discrepancy may be traced to the structural differences of the MAX phase (which is the input for the CE model) and *i*-MAX phases, where the former has all atoms (V + Zr, Al, C) in hexagonal lattices while the latter combines honeycomb (for V), hexagonal (for Zr and C) and Kagomé-like (for Al) lattices. Furthermore, it has been demonstrated that the transformation from a hexagonal Al lattice to a Kagomé-like lattice significantly decrease the energy of the system [8]. This may explain why CE fails to predict the correct outcome in Ref. [31], since mixing of V and Zr was only considered on the hexagonal metal lattice and thus fails to capture the important lattice transformation of the Al lattice. Such discrepancy demonstrates that CE is not always an appropriate choice for studying the mixing of metals in MAX phases [31-35].

In this work, we apply both CE and CSP methods to search for low-energy structures within a quaternary material system. We select the Mo-Sc-Al-B as a model system, motivated by the recently discovered *i*-MAB phase $Mo_{4/3}Sc_{2/3}AlB_2$, comprised of in-plane chemical ordering of Mo and Sc. Additional motivation is the close resemblance with the discrepancies reported for the MAX phases investigated with CE [31] and the ordered *i*-MAX phases [8]. The question is if CE and/or CSP can be used to verify the synthesized $Mo_{4/3}Sc_{2/3}AlB_2$ ($R\bar{3}m$) compound discovered in Ref. [13] while covering the phase space thoroughly with greater efficiency.

We show herein that neither approach used separately gives satisfactory results and suggest a framework where CE and CSP is combined, for an efficient and reliable search of the energy landscape in the quest for low energy structures. Not only do we verify the stable and ordered *i*-MAB phase $Mo_{4/3}Sc_{2/3}AlB_2$ ($R\bar{3}m$), discovered in Ref. [13], when combining the two methodologies, but also show that CE fails to account for important transformation in lattices not part of the parameterization. Furthermore, we predict

$Sc_4Mo_2Al_3B_6$ ($R3m$) to be stable, $MoScAlB_2$ ($R3m$) to be close to stable and identify two new low-energy MAB phase structures, Sc_2AlB_2 ($Pmmm$) and Mo_2AlB_2 ($P4/mbm$).

Methods

Density functional theory calculations

All structural relaxations required for the cluster expansion and crystal structure predictions were performed within the density functional theory (DFT) framework, using the Perdew-Burke-Ernzerhof (PBE) generalized gradient approximation (GGA) to model the exchange correlation effects, and the all-electron projector augmented wave (PAW) method, as implemented in the Vienna Ab initio Simulation Package (VASP) version 5.4.1 [36-38]. A plane wave energy cutoff of 400 eV and a Monkhorst-Pack scheme to sample the Brillouin zone with a k-point density of $2\pi \times 0.04$ Å^{-1} was used. The chosen settings are motivated by the convergence tests performed in Ref. [39], exploring quaternary metal borides, which yields energies accurate enough for efficient probing of the energy landscape. All structures were relaxed at ambient pressure and 0 K.

Evaluation of phase stability

The thermodynamical phase stability is here in determined by the formation enthalpy calculated at 0 K. The formation enthalpy of a general MAB phase $M_zA_yB_z$ is calculated by comparing the energy of $M_zA_yB_z$ with respect to all possible linear combinations of competing phases within the $M-A-\mathrm{B}$ material system. The $(Mo_xSc_{1-x})_2AlB_2$ system considered herein is thus compared to all phases in the $\mathrm{Mo}-\mathrm{Sc}-\mathrm{Al}-\mathrm{B}$ material system. The set of most competing phases, also referred to the equilibrium simplex, is designed as the linear combination of competing phases constituting the minimum energy, which represents the most favourable decompositions within the quaternary system. The equilibrium simplex is obtained by solving

$$\min E_{cp}\left(b^{\mathrm{Mo}}, b^{\mathrm{Sc}}, b^{Al}, b^{\mathrm{B}}\right) = \sum_{i}^{n} x_i E_i, \qquad (1)$$

in which the left-hand side of Eq. (1) represent the equilibrium simplex energy for the given composition constraints b^{Mo}, b^{Sc}, b^{Al} and b^{B} of elements Mo, Sc, Al and B, respectively. The right-hand side denotes the set of linear combinations constructed of phase i with amount x_i and energy E_i. The formation enthalpy, ΔH_{cp}, is then calculated as

$$\Delta H_{cp}((\mathrm{Mo}_x\mathrm{Sc}_{1-x})_2\mathrm{AlB}_2) = E((\mathrm{Mo}_x\mathrm{Sc}_{1-x})_2\mathrm{AlB}_2) - \min E_{cp}\left(b^{\mathrm{Mo}}, b^{\mathrm{Sc}}, b^{Al}, b^{\mathrm{B}}\right), \quad (2)$$

where $E((\mathrm{Mo}_x\mathrm{Sc}_{1-x})_2\mathrm{AlB}_2)$ is the calculated energy of $(\mathrm{Mo_xSc_{1-x}})_2\mathrm{AlB_2}$ and E_{cp} is the energy of the equilibrium simplex. Furthermore, a phase is attributed as stable when $\Delta H_{cp} < 0$ whereas a phase with $\Delta H_{cp} > 0$ is considered not stable or at best metastable. The set of competing phases considered herein are obtained from databases such as OQMD [40, 41], Materials project [42] and Springer Materials [43]. The complete set of competing phases are found in Table S1 and the identified set of most competing phases for each considered composition is shown in Table S2.

Cluster expansion

In the cluster expansion (CE) method [18] the energy of a crystalline solid is a function of the underlying grid of atomic sites or atomic arrangement of a given lattice. The herein used cluster expansion model is formulated by the Cluster Expansion in Atomic Simulation environment (CLEASE) code [44]. A brief introduction to the CE formalism is found in supplementary material. The training set is constructed by 300 configurations which is motivated by the convergence of the cross validation (CV) score versus size of training set shown in Figure S2. The generated configurations for each CE model were constructed to consist of up to a maximum of nine unit-cells. First-, second-, third-, and forth-body clusters were considered with a maximum length obtained through convergence of the CV score. A comparison of l_1- and l_2-schemes is shown in Figure S1 and illustrates a qualitatively similar appearance of two schemes. The herein selected schema is the l_2-regularization scheme to determine the effective cluster interactions (ECI) due to an overall lower CV score in contrast to l_1. Further figures verifying the ECIs, and the predictability of the CE models are displayed within Figure S3 and S4.

Crystal structure prediction

All crystal structure prediction searches have employed the Universal Structure predictor: Evolutionary Xtallography (USPEX) code [17, 45] where evolutionary algorithms are used to find a set of most optimal crystal structures within a given system. USPEX have been used for CSP searches of ternary Mo-Al-B and Sc-Al-B systems and for the pseudo-ternary $(Mo_xSc_{1-x})_2AlB_2$ system. The ternary systems were initiated with 200 randomly generated structures whereas succeeding generations each contained 40 structures. The CSP search for the pseudo-ternary system, $(Mo_xSc_{1-x})_2AlB_2$, was carried out by a variable composition search based on 800 randomly generated initial structures followed by succeeding generations containing 100 structures each. 60 % of phases of lowest energy in each generation was used as inspiration for the succeeding generation. 40 % of each succeeding generation was generated by the heredity operator, 15 % with lattice mutations, 15 % with transmutation operations, 15 % with soft-mode mutations, and 15 % randomly.

Results

Crystal structure prediction for ternary systems

We initiate the search for low energy structures by performing CSP searches on the ternary end-compositions of the $(Mo_xSc_{1-x})_2AlB_2$ system, i.e., Sc_2AlB_2 and Mo_2AlB_2. The evolution of the CSP search performed on the two ternary systems is shown in Figure 1a-b where the formation enthalpy, using Eq. 2, is shown as function of number of generations. Corresponding low-energy structures obtained after 30 consecutive generations are displayed in Figure 1c-d. In addition, we also considered previous known M_2AB_2 crystal structures, i.e., the symmetries of Cr_2AlB_2 (*Cmmm*) taken from Ref [35] and Ti_2InB_2 ($P\bar{6}m2$) from Ref [13], which are displayed in Figure 1e-f. Note that these additional structures are also among the individual structures found in the CSP search but at higher energy.

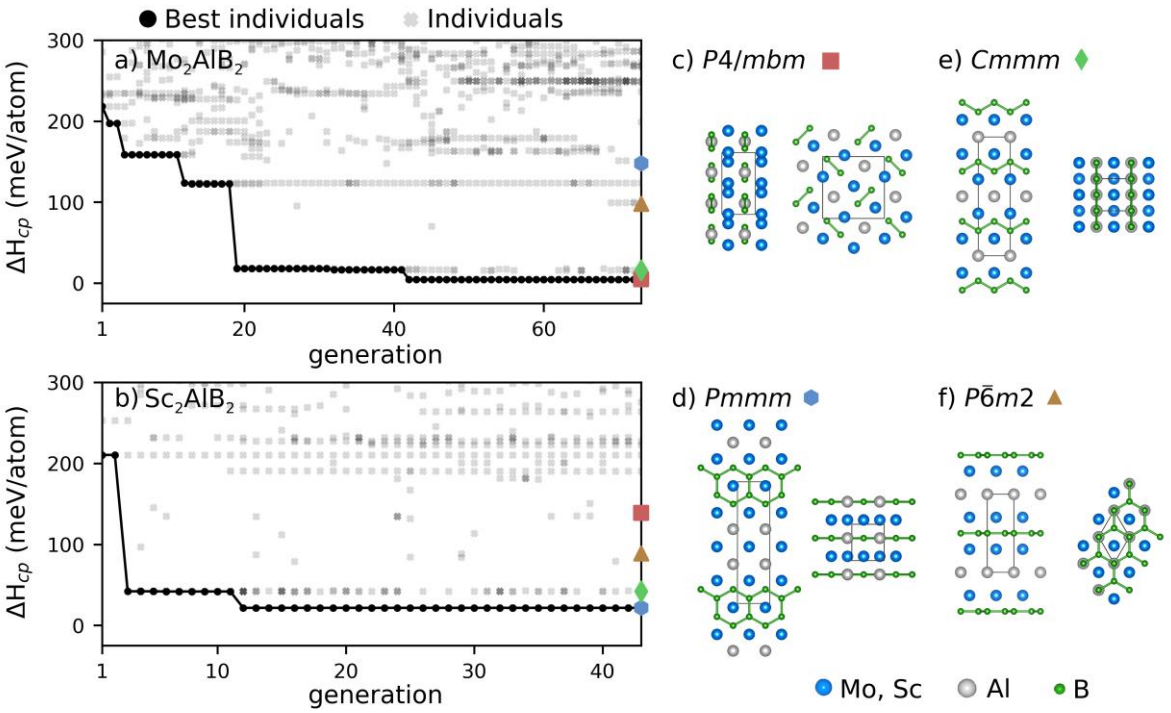

Figure 1. Formation enthalpy ΔH_{cp} of (a) Mo_2AlB_2 and (b) Sc_2AlB_2 along the evolutionary trajectory where lowest energy structure in each generation is represented by a black circle and those at higher energies by grey crosses. Schematic illustration of predicted crystal structures of lowest energy corresponding to (c) Mo_2AlB_2 in space group $P4/mbm$ and (d) Sc_2AlB_2 in space group $Pmmm$. Known M_2AB_2 prototype structures are illustrated with space group (e) $Cmmm$ and (f) $P\bar{6}m2$. Each structure is shown from two crystallographic different directions. Mo or Sc, Al, and B are represented by blue, grey, and green atoms.

For Mo_2AlB_2, displayed in Figure 1a, the predicted lowest crystal structure after 73 generations is $P4/mbm$, illustrated in Figure 1c, and it is close to stable with ΔH_{cp} = 5 meV/atom. This structure is obtained after 42 generations and have previously been reported for W_2CrB_2 in Ref. [21] with Mo/W and Al/Cr atoms in Wyckoff positions 4h and 2a, respectively, and originates from the V_3B_2 prototype structure. The structure found with next-lowest energy is $Cmmm$ (Figure 1e), i.e., the Cr_2AlB_2 prototype structure from Ref [46], at ΔH_{cp} = 16 meV/atom. Interesting to note is that the $Cmmm$ structure have been reported as intergrown in the stable MoAlB structure of $Cmcm$ symmetry [47]. Additionally, the $Pmmm$ (identified as the low-energy structure for Sc_2AlB_2 in Figure 1b and illustrated in Figure 1d)

and $P\bar{6}m2$ (based on Ti_2InB_2 from Ref [22] and illustrated in Figure 1f) structures are found at ΔH_{cp} = 148 and 89 meV/atom, respectively.

The evolution of the formation enthalpy for Sc_2AlB_2 is shown in Figure 1b and illustrates two close to stable low-energy structures of space group $Pmmm$ (Figure 1d) and $Cmmm$ (Figure 1e) at ΔH_{cp} = 22 and 42 meV/atom, respectively. The $Pmmm$ structure in Figure 1d is comprised of an extra arrangement of Sc-Al and Sc-B layers constituting to a layered B – Sc – B – Sc – Al – Sc – Al – Sc – Al – Sc – B – Sc – B stacking order. This is in contrast to the typical M_2AB_2 $Cmmm$ structure, shown in Figure 1e, with an Al – Sc – B – Sc – Al – Sc – B – Sc – Al stacking order. A noteworthy difference between the orthorhombic $Pmmm$ and $Cmmm$ and the hexagonal $P\bar{6}m2$ structures is the appearance of their B-layers which have a zig-zag structure for the former while being planar for the latter. Additionally, the $P4/mbm$ (identified as the low-energy structure for Mo_2AlB_2 in Figure 1a and illustrated in Figure 1c) and $P\bar{6}m2$ (Figure 1f) structures are found at ΔH_{cp} = 139 and 98 meV/atom, respectively. Detailed structural information related to structures shown in Figure 1c-f is found in Table 1.

Table 1. Space group, lattice parameters, Wyckoff position, and fractional atomic coordinates of predicted low-energy structures for Sc_2AlB_2 and Mo_2AlB_2 where x denotes the metallic ratio within the $(Mo_xSc_{1-x})_2AlB_2$, $0 \leq x \leq 1$, system.

x	Compound	Space group	ΔH_{cp} (meV/atom)	Lattice parameters (Å)	Atom (Wyckoff site)	Fractional coordinates		
						x	y	z
0	Sc_2AlB_2	*Pmmm*	22	a = 3.20505 Å	Sc1 (1a)	0.00000	0.00000	0.00000
				b = 3.54197 Å	Sc2 (2q)	0.00000	0.00000	0.27859
				c = 11.96331 Å	Sc3 (1d)	0.50000	0.00000	0.50000
					B1 (2r)	0.00000	0.50000	0.42464
					B2 (2t)	0.50000	0.50000	0.35200
					Al (2t)	0.50000	0.50000	0.14324
0	Sc_2AlB_2	*P4/mbm*	139	a = 6.15293 Å	Al (2b)	0.00000	0.00000	0.50000
				c = 3.55744 Å	B (4h)	0.59840	0.09840	0.50000
					Sc (4g)	0.17764	0.67764	0.00000
0	Sc_2AlB_2	*Cmmm*	42	a = 11.81834 Å	Al (2a)	0.00000	0.00000	0.00000
				b = 3.18704 Å	B (4g)	0.21530	0.00000	0.00000
				c = 3.59432 Å	Sc (4h)	0.35903	0.00000	0.50000
0	Sc_2AlB_2	*P$\bar{6}$m2*	98	a = 3.14487 Å	Al (1a)	0.00000	0.00000	0.00000
				c = 8.43732 Å	B1 (1b)	0.00000	0.00000	0.50000
					B2 (1f)	0.66667	0.33333	0.50000
					Sc (2h)	0.33333	0.66667	0.29726
1	Mo_2AlB_2	*Pmmm*	148	a = 3.05299 Å	Mo1 (1a)	0.00000	0.00000	0.00000
				b = 3.18052 Å	Mo2 (2q)	0.00000	0.00000	0.28063
				c = 11.66041 Å	Mo3 (1d)	0.50000	0.00000	0.50000
					B1 (2r)	0.00000	0.50000	0.42213
					B2 (2t)	0.50000	0.50000	0.34062
					Al (2t)	0.50000	0.50000	0.13401
1	Mo_2AlB_2	*Cmmm*	16	a = 11.63432 Å	Al (2a)	0.00000	0.00000	0.00000
				b = 3.08914 Å	B (4g)	0.20781	0.00000	0.00000
				c = 3.12544 Å	Mo (4h)	0.35717	0.00000	0.50000

1	Mo_2AlB_2	$P\bar{6}m2$	89	a = 3.04865 Å c = 7.35579 Å	Al (1a) B1 (1b) B2 (1f) Mo (2h)	0.00000 0.00000 0.66667 0.33333	0.00000 0.00000 0.33333 0.66667	0.00000 0.50000 0.50000 0.29350
1	Mo_2AlB_2	*P4/mbm*	5	a = 5.89216 Å c = 3.16159 Å	Al (2b) B (4h) Mo (4g)	0.00000 0.61133 0.17420	0.00000 0.11133 0.67420	0.50000 0.50000 0.00000

Cluster expansion for identification of mixing tendencies

The search for low-energy structures within the $(Mo_xSc_{1-x})_2AlB_2$ system is continued as low-energy symmetries within the Mo_2AlB_2 and Sc_2AlB_2 systems have been identified using CSP in addition to the collected known M_2AB_2 compositions found in related systems. Initially, we aim to reveal the alloying tendencies in the $(Mo_xSc_{1-x})_2AlB_2$ system by designing CE models based on the four collected space group symmetries $Pmmm$, $P4/mbm$, $Cmmm$, and $P\bar{6}m2$. The Al and B sublattices are considered as spectator atoms as the alloying is focused on the metal lattice. The lattice constants used to construct the CE models for each considered symmetry were set to an average value of the relaxed Mo_2AlB_2 and Sc_2AlB_2 compositions. A database of different configurations σ of $(Mo_xSc_{1-x})_2AlB_2$ alloys were initially established for each considered CE model. Each CE model contained a training set comprised of 300 structures whose configurations were used to predict the energy for at least 5,000 unique structures. Figure 2a-d shows the isostructural formation enthalpy ΔH_{iso} as function of x in $(Mo_xSc_{1-x})_2AlB_2$ for the DFT training set and CE predicted structures. Here we use ΔH_{iso} to illustrate possible mixing tendencies among the four model systems. In addition, the stability of each CE model is shown in Figure 2e-h.

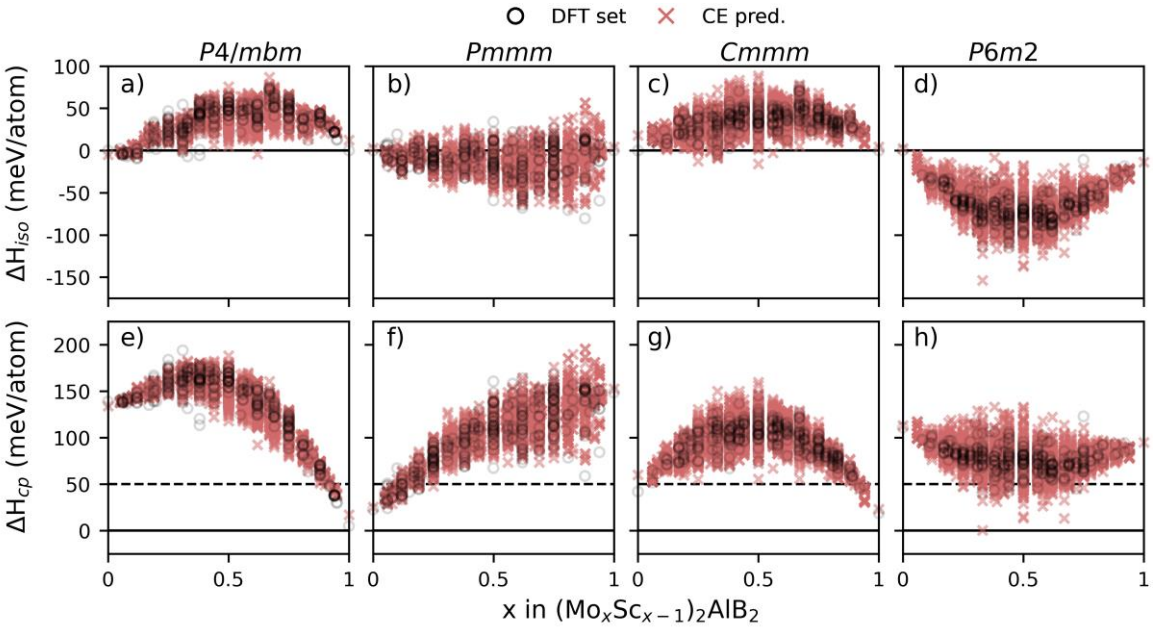

Figure 2. (a-d) Isostructural formation enthalpy ΔH_{iso} and (e-f) formation enthalpy ΔH_{cp} of $(Mo_xSc_{1-x})_2AlB_2$ based on M_2AlB_2 in the (a, e) $P4/mbm$, (b, f) $Pmmm$, (c, g) $Cmmm$, and (d, h) $P\bar{6}m2$ crystal structure where M = Sc, Mo. The training set is represented by black circles and the predicted phases by red crosses. The dashed horizontal line in (e-h) represent the stability cutoff.

Neither $P4/mbm$ (Figure 2a) nor $Cmmm$ (Figure 2c) is found to have any preference for mixing Mo and Sc on the M-site, as indicated by $\Delta H_{\mathrm{iso}} > 0$. This in contrast to $Pmmm$ (Figure 2b) and $P\bar{6}m2$ (Figure 2d) which both show mixing tendencies as concluded from most of the predicted CE structures being found with $\Delta H_{\mathrm{iso}} < 0$. This is most pronounced for the hexagonal $P\bar{6}m2$ model system.

The stability of the predicted phases for the four model systems is obtained by applying Eq. 2. This is illustrated in Figure 2e-h where the formation enthalpy ΔH_{cp} is shown as function of x in $(Mo_xSc_{1-x})_2AlB_2$. The no-mixing tendencies displayed for $P4/mbm$ (Figure 2e) and $Cmmm$ (Figure 2g) is now even more apparent. For the $Pmmm$ symmetry in Figure 2f, the Mo-rich region, which in Figure 2b demonstrated mixing tendencies, is now far from stable. For the $P\bar{6}m2$ CE model, a few phases are predicted to be close to stable, e.g., x = 0.33, 0.5 and 0.67 with $\Delta H_{\mathrm{cp}} = 5$, 14 and 7 meV/atom, respectively. Moreover, within the $P\bar{6}m2$ model system there is a range of additional structures of low energy.

A cutoff set to $\Delta H_{\mathrm{cp}} < 50$ meV/atom is introduced in order to limit the number of structures chosen for further investigation. The CE models based on the $P4/mbm$, $Pmmm$, and $Cmmm$ are thus sorted out as they all have predicted quaternary $(Mo_xSc_{1-x})_2AlB_2$ structures located above the assigned cutoff or is below the cutoff but close to a ternary end-point. In the $P\bar{6}m2$ model system there are 105 CE-predicted structures located beneath the cutoff, shown in Figure 2h. Here we note that the hexagonal $P\bar{6}m2$ do resemble the hexagonal MAX phases for which there is a discrepancy between experimental findings of $(V_{2/3}Zr_{1/3})_2AlC$ with in-plane order while CE predicts phase segregation into V_2AlC and Zr_2AlC. We therefore choose to further relax all these 105 structures using DFT in order to reveal if such discrepancies also apply for the herein studied $P\bar{6}m2$ CE model. Figure 3a shows the predicted energies of the CE model (red crosses) along with corresponding relaxed DFT energies (blue circles) for the 105 structures.

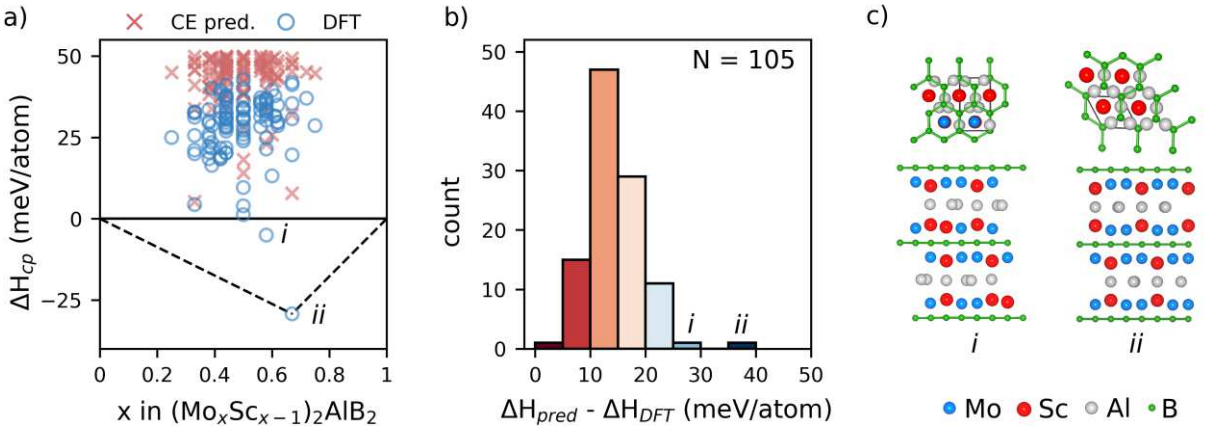

Figure 3. (a) Calculated ΔH_{cp} for x in $(Mo_xSc_{1-x})_2AlB_2$ upon relaxation of the 105 CE-predicted structures with ΔH_{cp} < +50 meV/atom in Figure 2h where open blue circles represent relaxed structures and red crosses CE-predicted structures. (b) Distribution of the energy difference between predicted CE structures and corresponding relaxed structures depicted in (a). (c) Schematic illustration of the two structures whose CE-predicted energy differs significantly from their DFT relaxed energy, $\Delta H_{pred} - \Delta H_{DFT} > 25$ meV/atom.

Two of the structures appear stable, with $\Delta H_{\mathrm{cp}} < 0$ meV/atom, after relaxation. $Mo_7Sc_{12}Al_6B_{12}$ (marked *i* with space group $P1$ in Figure 3c) and $Mo_4Sc_2Al_3B_6$ (marked *ii* with space group $R32$ in Figure 3c),

with ΔH_{cp} = -5 and -29 meV/atom, respectively. $Mo_4Sc_2Al_3B_6$ is similar to the predicted and synthesized in-plane ordered $Mo_{4/3}Sc_{2/3}AlB_2$ ($R\bar{3}m$) in Ref [13] with a formation enthalpy $\Delta H_{cp} = -30$ meV/atom.

The validity of the predicted energies for all configurations is further studied as the chemical ordering may impact neighbouring spectator lattices not considered within the CE model, e.g., change of Al-lattice in *i*-MAX phases [8]. The energy difference between the predicted formation enthalpies and DFT enthalpies, shown in Figure 3b, illustrates that energy of all 105 configurations decrease upon relaxation with a mean decrease of ~13 meV/atom. However, the two predicted stable configurations, $Mo_7Sc_{12}Al_6B_{12}$ at $x = 0.54$ and $Mo_4Sc_2Al_3B_6$ at $x = 0.67$, both displays the largest energy difference between predicted and relaxed with a change of 28 and 37 meV/atom, respectively. In order to enlighten this discrepancy, we performed a stepwise displacement, denoted as Δz, of the Sc atoms towards the Al lattice for the CE-predicted $Mo_4Sc_2Al_3B_6$ structure at $x = 0.67$ while observing the change in energy. This was performed for four different relaxation constraints; with a fixed unit cell and (i) all atoms kept fixed, (ii) with only Mo allowed to rearrange, (iii) with only Al allowed to rearrange, (iv) with Mo, Al and B are allowed to rearrange or (V) with a complete relaxation of the unit cell where all atoms are allowed to rearrange. A schematic illustration of these five cases is shown in Figure 4a for Δz = 1.5 %.

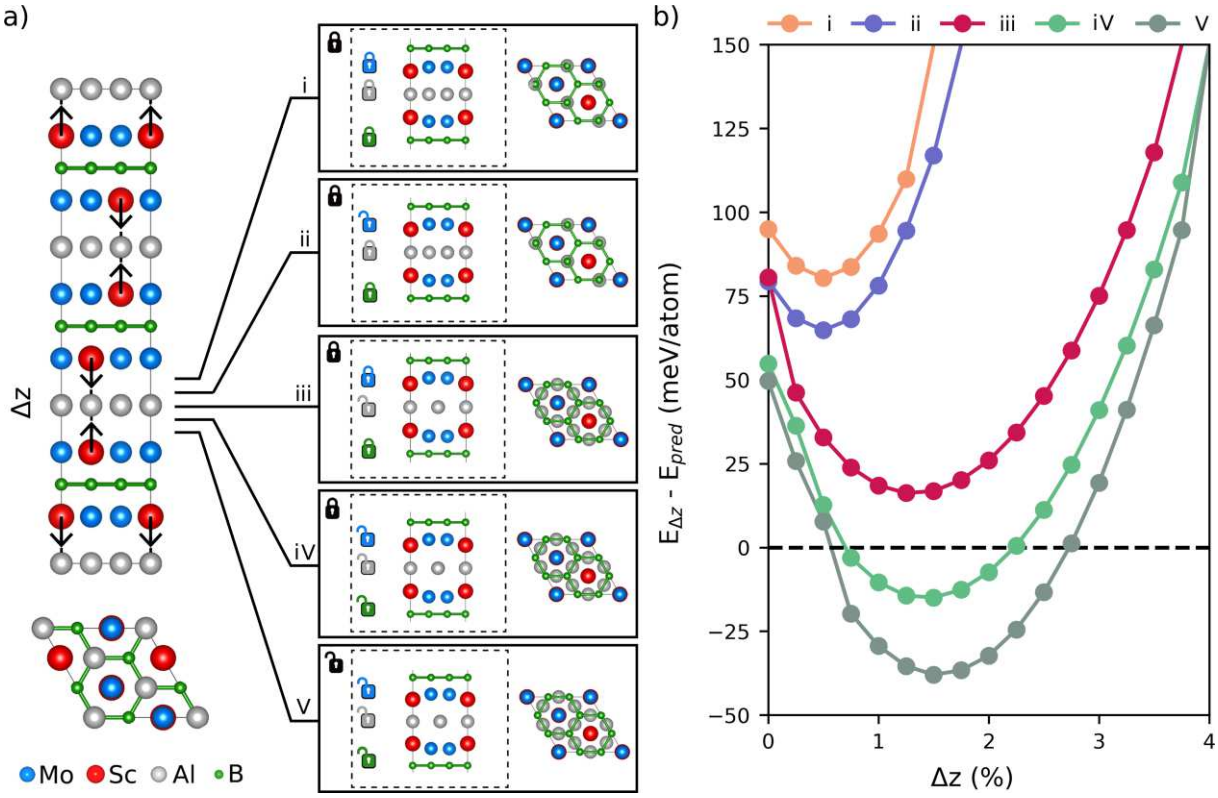

Figure 4 (a) A schematic overview of the manual rearrangement of Sc towards the Al-layer within the predicted $R32$ symmetry where (i), (ii), (iii), (iv) and (v) illustrates the considered constraints where Mo, Sc, Al and B are represented by blue, red, grey, and green atoms. (b) Relative energy for the considered constraints as Sc is moved towards the Al-layer in steps of 1 % of the c-axis notated as Δz.

The change in energy upon the stepwise displacement of the Sc atoms is shown in Figure 4b in respect to the CE-predicted energy of $Mo_4Sc_2Al_3B_6$. The predicted energy of $Mo_4Sc_2Al_3B$ is observed be closest to the relaxed structures in cases (iii) and (iv) despite being structurally equivalent with case (i) at Δz = 0. Both case (i) and (ii) illustrates that an energy decrease is achieved upon displacing Sc towards the Al-layer up to Δz = 1 %. However, a much greater decrease in energy is found for cases (iii), (iv) and (v) when the Al-layer is allowed to relax in-plane. The Al-layer is observed in cases (iii), (iv) and (v) to rearrange from a hexagonal to a Kagomé lattice which significantly lowers the energy. The lowest energy is found for case (v) where both the unit cell and the atoms are allowed to relax upon displacing Sc towards the Al-lattice. An energy difference of -37 meV/atom for the 1.5 % displacement of Sc is observed, which is in agreement with the energy difference demonstrated in Figure 3b.

The major component of the decreased energy is thus traceable to the rearrangement of the Al atoms caused by the displacement of Sc towards the Al layer. Minor energy contributions are found from the Mo, B and structural relaxations. Such secondary effects in spectator lattices are in agreement with similar observations demonstrated for the *i*-MAX phases in Ref [48]. There, metals (M' and M'') with a significant size difference ($r_{M'} > r_{M''}$) in a ratio M':M' = 2:1 are mixed within the layered hexagonal MAX phase, which forces the larger M' to be displaced towards the Al-layer. This procedure is illustrated in Figure 4 where the Al lattice is observed to rearrange from a hexagonal lattice, which is the spectator lattice used within the CE model for the $P\bar{6}m2$ symmetry, to a Kagomé lattice as Sc is displaced towards the Al-layer. The missing 37 meV/atom for the predicted CE configuration is thus assigned to the two principal factors: (1) having Sc and Mo in the same layer and (2) Al in a hexagonal lattice.

The above results exemplify the limitations of using CE for prediction of low-energy structures for model systems where inherent chemical ordering, as in both structures displayed in Figure 3c, may impact nearby lattices not part of the cluster expansion parametrization. The parametrization may thus not be completely reliable, which motivates post-relaxation of CE-predicted configurations. The CE models demonstrated in Figures 3 are dependent on and limited by their model input structures. The generated ECIs are thus only valid for the metal lattice on which the mixing of Mo and Sc is performed. Events such as structural transformation occurring within a nearby spectator lattice can thus not be modelled, and its impact on the energy may thus be missed. This is the case for both $Mo_7Sc_{12}Al_6B_{12}$ and $Mo_4Sc_2Al_3B_6$, being predicted with energies 25 and 37 meV/atom, respectively, larger than their relaxed DFT energies (see overview in Figure 3b). Similar observations have also been demonstrated for $(V_{2/3}Zr_{1/3})_2AlC$ *i*-MAX phase [8]. These secondary effects are more significant within $Mo_4Sc_2Al_3B_6$ which is shown in Figure 4. An alternative approach which circumvents this problem, and where the dependence of any initial structure is of lesser importance or even neglected, is needed.

Search for low-energy structures in a quaternary system

Next, we focus on exploring the chemical phase space within the quaternary $(Mo_xSc_{1-x})_2AlB_2$ system where $0 \leq x \leq 1$ through use of the crystal structure prediction code USPEX. The aim is to identify stable low-energy structures. Figure 5a illustrates the evolution of the CSP search where the formation enthalpy, using Eq. 2, is shown as a function of number of generations for x = 2/3 without (black) and with seeds applied after 5 (red), 25 (blue), and 50 (yellow) generations. Included seed structures are gathered from relaxed CE-predicted structures in Figure 3a.

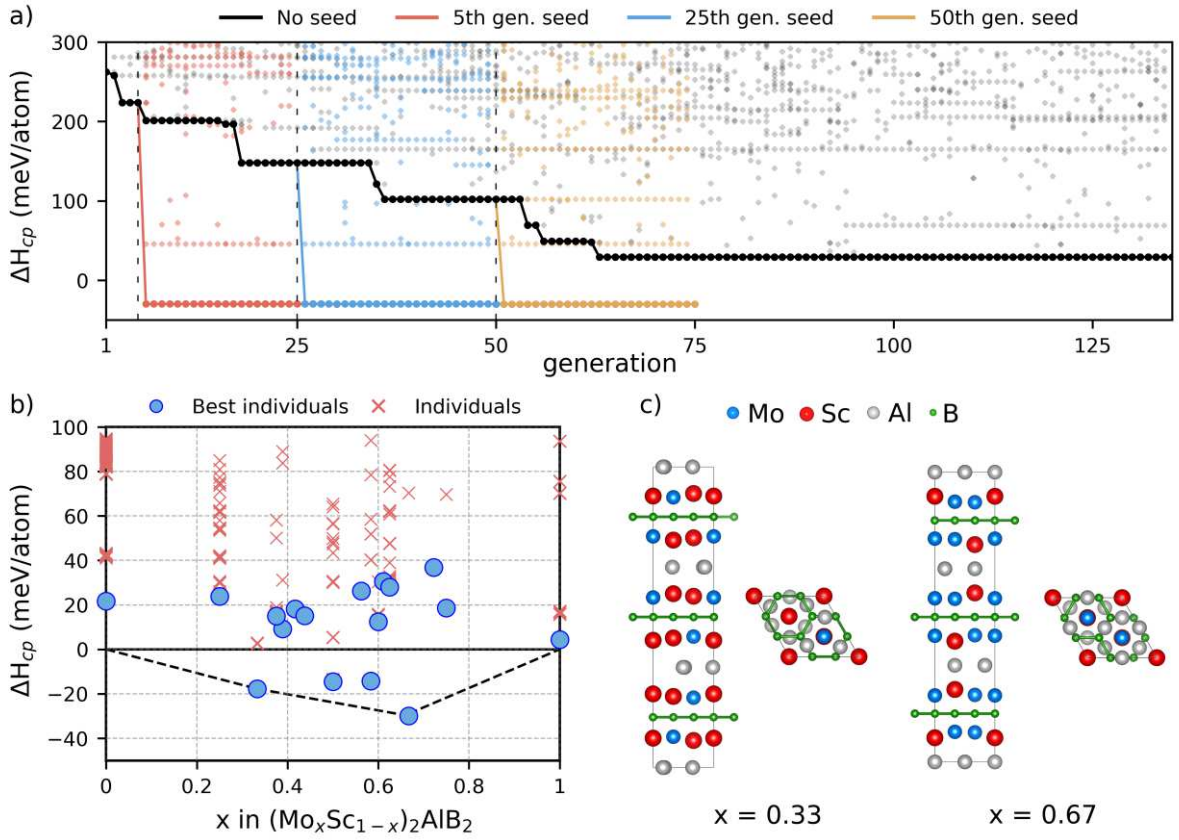

Figure 5. (a) Formation enthalpy ΔH_{cp} of $(Mo_xSc_{1-x})_2AlB_2$, x = 2/3, along the evolutionary trajectory without (black) and with seed structures applied after 5 (red), 25 (blue) and 50 (yellow) generations. (b) ΔH_{cp} as function of x in $(Mo_xSc_{1-x})_2AlB_2$ for predicted low-energy structures when performing the variational composition search. (c) Schematic illustration of the predicted stable structures located at x = 0.33 and x = 0.67 from two directions.

Figure 5a illustrates the formation enthalpy, ΔH_{cp}, for x = 2/3 along the evolutionary trajectory. When no seeds are used, the predicted lowest-energy structure after 135 generations is found not stable, with $\Delta H_{cp} = 29$ meV/atom, corresponding to a structure with orthorhombic $Amm2$ space group symmetry. This structure is illustrated in Figure S6a, with structural information in Table S3, resembling the orthorhombic $Cmmm$ and $Pmmm$ structures but with double-layers of Al and Mo. This can be compared to the evolutionary searches using seeds from relaxed CE-predicted structures in Figure 3a. Every seed-inspired CSP search results in a predicted stable structure, ΔH_{cp} = -30 meV/atom, with space group $R\bar{3}m$. This structure is found immediately after applying seeds following 5, 25 and 50 generations. It should be noted that the number of individual structures generated with lower energy is observed to increase when seeds are applied for a later generation. From this we can conclude that using seeds not only predicts lower-energy structures, but also significantly reduces the number of generations required to find potential low energy structures.

Using seed structures acquired from the CE predictions, we performed a variable composition search within the quaternary $(Mo_xSc_{1-x})_2AlB_2$ system for $0 \leq x \leq 1$. Figure 5b shows the corresponding formation enthalpy ΔH_{cp} as function of x but only for $\Delta H_{\mathrm{cp}} < 100$ meV/atom. Additional results including structures with $\Delta H_{\mathrm{cp}} < 300$ meV/atom is shown in Figure S5. The lowest energy structures for each composition x are indicated by a filled blue circle and those above by red crosses. Two structures are found to be stable at x = 1/3 and 2/3, corresponding to $Mo_2Sc_4Al_3B_6$ ($R3m$) and $Mo_4Sc_2Al_3B_6$ ($R\bar{3}m$) with ΔH_{cp} being -18 and -30 meV/atom, respectively. Additional and similar structures with $\Delta H_{cp} < 0$ are found at x = 0.5 and 0.54 and are referred to as meta-stable. Schematic illustration of here identified stable structures are shown in Figure 5c and the additional meta-stable low-energy structures in Figure S6.

Common for the low-energy structures at x = 1/3, 1/2 and 2/3, displayed in Figure 5c and Figure S5, are the flat Al-layers interleaved with M-B layers. The $Mo_4Sc_2Al_3B_6$ composition demonstrates a more symmetric characteristics with Sc located closer to the Al-layer while Mo is closer to the B-layer. $Mo_2Sc_4Al_3B_6$ and $Mo_3Sc_3Al_3B_6$, on the other hand, yield less symmetric metal-layers which is likely the

reason for not being as stable as the predicted $Mo_4Sc_2Al_3B_6$ phase. Additional structural information for the $\Delta H_{cp} < 0$ structures predicted with CSP is found in Table 2.

Table 2 Space group, lattice parameters, Wyckoff position, and fractional atomic coordinates of predicted low-energy structures within the $(Mo_xSc_{1-x})_2AlB_2$, $0 \leq x \leq 1$, system.

x	Compound	Space group	ΔH_{cp} (meV/atom)	Lattice parameters (Å)	Atom (Wyckoff site)	Fractional coordinates		
						x	y	z
1/3	$Sc_4Mo_2Al_3B_6$	*R*3	-18	a = 5.42213 Å	Mo1 (3a)	0.00000	0.00000	0.56565
				c = 23.28442 Å	Mo2 (3a)	0.00000	0.00000	0.76901
					Sc1 (3a)	0.00000	0.00000	0.42328
					Sc2 (3a)	0.00000	0.00000	-0.09684
					Sc3 (3a)	0.00000	0.00000	0.09768
					Sc4 (3a)	0.00000	0.00000	0.24499
					Al (9b)	0.34849	0.18693	0.00066
					B1 (9b)	0.00214	0.66859	0.16730
					B2 (9b)	0.66665	0.66878	0.16729
1/2	$MoScAlB_2$	*Cmcm*	-14	a = 15.03898 Å	Mo1 (8g)	0.34446	0.12533	0.25000
				b = 6.34981 Å	Sc1 (8g)	0.13332	0.14946	0.25000
				c = 5.36435 Å	Al1 (4b)	0.00000	0.50000	0.00000
					Al2 (4c)	0.00000	0.85254	0.25000
					B (16h)	0.24641	0.12202	0.58048
7/13	$Mo_7Sc_5Al_6B_{12}$	*Pm*	-14	a = 8.13509 Å	Mo1 (1b)	0.68712	0.50000	0.39685
				b = 5.39719 Å	Mo2 (1b)	0.30743	0.50000	0.60235
				c = 9.33792 Å	Mo3 (1b)	0.69413	0.50000	0.73741
				β = 112.50750 °	Mo4 (1b)	0.30809	0.50000	-0.05799
					Mo5 (1a)	0.30259	0.00000	0.10538
					Mo6 (1a)	0.69335	0.00000	0.22860
					Mo7 (1a)	0.31091	0.00000	0.43564
					Sc1 (1b)	0.74168	0.50000	0.08382
					Sc2 (1b)	0.25604	0.50000	0.25511
					Sc3 (1a)	0.74871	0.00000	0.58056
					Sc4 (1a)	0.25173	0.00000	0.75152
					Sc5 (1a)	0.70860	0.00000	-0.09430
					Al1 (2c)	0.01086	0.25518	-0.08558
					Al2 (2c)	-0.00125	0.24863	0.42252
					Al3 (1b)	-0.00254	0.50000	0.66556
					Al4 (1a)	0.01144	0.00000	0.18021
					B1 (2c)	0.49911	0.66690	0.16787
					B2 (2c)	0.50077	0.66781	0.50196
					B3 (2c)	0.49583	0.66804	0.83440
					B4 (2c)	0.49688	0.16692	-0.00063
					B5 (2c)	0.50150	0.16670	0.33641
					B6 (2c)	0.49781	0.16425	0.66802
2/3	$Mo_4Sc_2Al_3B_6$	$R\bar{3}m$	-30	a = 5.37013 Å	Mo1 (6c)	0.00000	0.00000	0.22946
				c = 22.44751 Å	Mo2 (6c)	0.00000	0.00000	0.43535
					Sc (6c)	0.00000	0.00000	0.08320
					Al (9e)	0.50000	0.00000	0.00000
					B (18g)	0.66519	0.00000	0.50000

Combining cluster expansion and crystal structure prediction

Using either cluster expansion (CE) or crystal structure prediction (CSP) alone when searching for low-energy structures in multi-component system, like the quaternary Mo-Sc-Al-B system, may yield limited and inadequate results. Even though CE is the less computationally demanding out of the two approaches, it can be limited by the model structure which may yield a mismatch in predicted energies due to, e.g., secondary effects in spectator lattices which cannot be captured by the expansion. CSP

searches, on the other hand, are independent on any initial structure but are more demanding, where each USPEX run consists of an initial sampling of up to 200 DFT calculations followed by at least 50 generations, where each generation is comprised of 40 individual DFT calculations, before reaching proper convergence. It may even give a structure which is not of low energy as demonstrated in Figure 5a. Furthermore, performing a variable composition search is even more demanding, which herein consisted of 800 initially sampled structures with at least 50 generations, each containing 100 new structures.

The herein suggested solution for performing an efficient search in the quest for low-energy structures within a multi-component system is to combine CE and CSP. A proposed framework is illustrated in Figure 6 for studying mixing and/or stability within higher order systems, such as the quaternary $(Mo_xSc_{1-x})_2AlB_2$ system considered in this work.

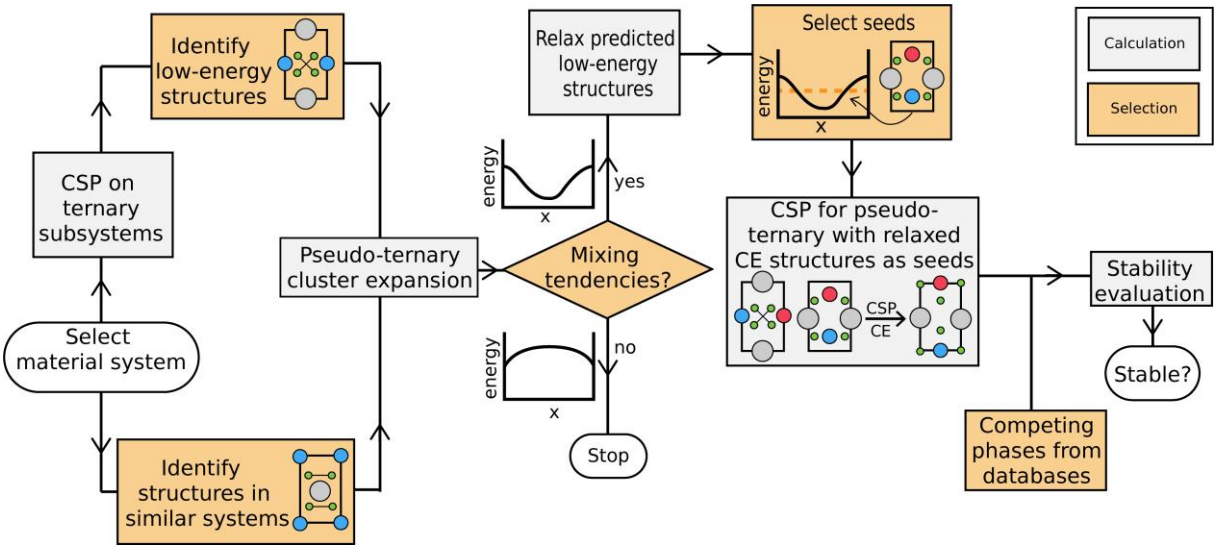

Figure 6. Schematic representation of the process combining cluster expansion with crystal structure prediction. Grey labels represent computational procedures whereas yellow labels denote sections which require manual input.

Before constructing the CE model systems, a CSP search should be performed on the lower order systems constituting the system in focus, in our case Mo_2AlB_2 and Sc_2AlB_2, to identify possible low-energy structures to be used for constructing the CE models. These structures do not necessarily have to be stable, as exemplified herein for $P4/mbm$ Mo_2AlB_2 and $Pmmm$ Sc_2AlB_2. In addition, a literature

search for structures in similar ternary system is also recommended. In this work such structures correspond to $Cmmm$ Cr_2AlB_2 and $P\bar{6}m2$ Ti_2InB_2. Next, CE models are constructed based on the identified ternary low-energy structures. The predicted structures from the CE models allows for the possibility to decide if there are any mixing tendencies. This analysis can be performed both in terms of isostructural enthalpy, ΔH_{iso}, and with respect to competing phases by calculating the formation enthalpy ΔH_{cp}. Systems identified with no indication of mixing and/or stability tendencies are discarded. CE model systems showing tendencies towards mixing, i.e., $\Delta H_{\mathrm{iso}} < 0$, and where the structures are close to stable are selected for further investigation by performing DFT computations. These structures are later used as seeds when performing a final CSP search on the quaternary, or higher ordered, system.

Discussion

Approaches like crystal structure prediction and cluster expansion are in general useful methods for predicting low energy crystal structures. CE offers a robust, and computationally effortless procedure as the energies of generated crystal structures is predicted by mapping the cluster interactions of a training set onto a lattice of mixed atomic species. The model relies on a predefined lattice where mixing is to take place, but where important aspects may be overlooked, such as rearrangement in neighbouring spectator lattices, as demonstrated herein for the hexagonal and layered $P\bar{6}m2$ model system and elsewhere for specific MAX phase compositions. Additional work is needed to reveal if this is a problem for layered hexagonal materials in general. CE also only covers the specific symmetries considered, which herein are the hexagonal, tetragonal, and orthorhombic models of M_2AB_2 structures, and thus only explores a fraction of the complete energy landscape. Also note that the effective interactions can, as in the case of the CE-predicted $Mo_4Sc_2Al_3B_6$ ($P\bar{6}m2$) structure, fail to mimic important structural transformation due to the mixing of metals of a significant size difference. This explains the here obtained 37 meV/atom energy difference between the predicted CE structure and the relaxed one. Still, a CE model could potentially serve as good seed generator for the CSP search. With seeds from CE added to the CSP search we find multiple crystal symmetries at various compositions in $(Mo_xSc_{1-x})_2AlB_2$, from orthorhombic and tetragonal symmetries at the ternary end-points ($x = 0$ and 1) to trigonal, orthorhombic, and monoclinic symmetries in between.

Even though the crystal structure prediction algorithms utilized in USPEX provides a strong framework, covering the complete energy landscape of a quaternary system is a daunting task as the complexity rapidly increases as compared to a ternary system. Even if we limit our search for low energy crystal structures to the quaternary $(Mo_xSc_{1-x})_2AlB_2$ system, the variety of possible structures becomes extremely large. Here we show that CE combined with CSP could accelerate the search for low-energy structures by utilizing the strengths of both frameworks.

We suggest that the combination of the two methodologies, CE + CSP, could reduce the computational demands while still searching the energy landscape of the considered material system thoroughly and efficiently, for identification of low-energy structures. The CE model offers a computational effortless framework covering the initial grounds of the system which may later be used as seed structures to further inspire the evolution of the CSP search.

Conclusions

We have herein investigated the mixing of metals within the quaternary $(Mo_xSc_{1-x})_2AlB_2$ system by combining cluster expansion and crystal structure prediction with DFT calculations. From CSP searches of Sc_2AlB_2 and Mo_2AlB_2 we identified four model systems for constructing the cluster expansion, including one tetragonal, two orthorhombic, and one hexagonal symmetry structure. From CE-predictions, apparent mixing tendencies were only found for the hexagonal model system. However, CE fail to account for secondary effects within the spectator Al lattice. To circumvent this problem, low-energy CE-predicted structure are instead used as seeds for a CSP search within the $(Mo_xSc_{1-x})_2AlB_2$ system. By using seeds structures, we are able to identify the stable $Mo_{4/3}Sc_{2/3}AlB_2$ ($R\bar{3}m$), previously referred to as *i*-MAB, comprised of chemical ordering of Mo and Sc, to be stable. The CSP searches is demonstrated to discover low-energy phases more efficiently when inspired by seed structures. The proposed framework of combining the CE formulism with CSP methods cancels out the limitations of each framework (CE being limited to a specific lattice and the great computational demands by CSP) and offers an efficient and thoroughly approach when searching for novel stable multi-component materials.

Competing interests

The authors declare no competing financial or non-financial interests.

Data availability

The authors declare that all data supporting the results of this study are available from the corresponding author upon request.

Author contributions

The project was conceptualized by A.C and M.D. The ab initio simulations were carried out by A.C under supervision by M.D. All authors contributed to the discussion and the writing of the paper and approved the final version of the manuscript.

Acknowledgements

M.D. acknowledges support from the Swedish Research council through project 2019-05047. J. R. acknowledges funding from the Knut and Alice Wallenberg (KAW) Foundation for a Fellowship/Scholar Grant and Project funding (KAW 2020.0033). The calculations were carried out using supercomputer resources provided by the Swedish National Infrastructure for Computing (SNIC) at the National Supercomputer Center (NSC) and the High Performance Computing Center North (HPC2N), partially founded by the Swedish Research Council through grant agreement no. 2018-05973.

References

1. Villars, P. and S. Iwata, *Pauling File verifies/reveals 12 principles in materials science supporting four cornerstones given by Nature.* Chemistry of metals and alloys, 2013(6,№ 3-4): p. 81-108.
2. Sun, W., et al., *A map of the inorganic ternary metal nitrides.* Nat Mater, 2019. **18**(7): p. 732-739.
3. Dahlqvist, M., et al., *Out-Of-Plane Ordered Laminate Borides and Their 2D Ti-Based Derivative from Chemical Exfoliation.* Advanced Materials, 2021. **33**(38): p. 2008361.

4. Sokol, M., et al., *On the Chemical Diversity of the MAX Phases.* Trends in Chemistry, 2019. **1**(2): p. 210-223.

5. Barsoum, M.W., *The $M_{N+1}AX_N$ phases: A new class of solids: Thermodynamically stable nanolaminates.* Progress in Solid State Chemistry, 2000. **28**(1): p. 201-281.

6. Naguib, M., et al., *Two-Dimensional Nanocrystals Produced by Exfoliation of Ti_3AlC_2.* Advanced Materials, 2011. **23**(37): p. 4248-4253.

7. Vahid Mohammadi, A., J. Rosen, and Y. Gogotsi, *The world of two-dimensional carbides and nitrides (MXenes).* Science, 2021. **372**(6547): p. eabf1581.

8. Dahlqvist, M., et al., *Prediction and synthesis of a family of atomic laminate phases with Kagomé-like and in-plane chemical ordering.* Science Advances, 2017. **3**(7): p. e1700642.

9. Tao, Q., et al., *Two-dimensional Mo1.33C MXene with divacancy ordering prepared from parent 3D laminate with in-plane chemical ordering.* Nat Commun, 2017. **8**: p. 14949.

10. Meshkian, R., et al., *W-Based Atomic Laminates and Their 2D Derivative W1.33 C MXene with Vacancy Ordering.* Adv Mater, 2018. **30**(21): p. e1706409.

11. Ahmed, B., A.E. Ghazaly, and J. Rosen, *i-MXenes for Energy Storage and Catalysis.* Advanced Functional Materials, 2020. **30**(47).

12. Persson, I., et al., *Tailoring Structure, Composition, and Energy Storage Properties of MXenes from Selective Etching of In-Plane, Chemically Ordered MAX Phases.* Small, 2018. **14**(17): p. e1703676.

13. Dahlqvist, M., et al., *Theoretical Prediction and Synthesis of a Family of Atomic Laminate Metal Borides with In-Plane Chemical Ordering.* Journal of the American Chemical Society, 2020. **142**(43): p. 18583-18591.

14. Zhou, J., et al., *Boridene: Two-dimensional $Mo_{4/3}B_{2-x}$ with ordered metal vacancies obtained by chemical exfoliation.* Science, 2021. **373**(6556): p. 801-805.

15. Oganov, A.R. and C.W. Glass, *Crystal structure prediction using ab initio evolutionary techniques: Principles and applications.* The Journal of Chemical Physics, 2006. **124**(24): p. 244704.

16. Oganov, A.R., A.O. Lyakhov, and M. Valle, *How Evolutionary Crystal Structure Prediction Works—and Why.* Accounts of Chemical Research, 2011. **44**(3): p. 227-237.

17. Lyakhov, A.O., et al., *New developments in evolutionary structure prediction algorithm USPEX.* Computer Physics Communications, 2013. **184**(4): p. 1172-1182.

18. Sanchez, J.M., F. Ducastelle, and D. Gratias, *Generalized cluster description of multicomponent systems.* Physica A: Statistical Mechanics and its Applications, 1984. **128**(1): p. 334-350.

19. Rybkovskiy, D.V., et al., *Structure, Stability, and Mechanical Properties of Boron-Rich Mo–B Phases: A Computational Study.* The Journal of Physical Chemistry Letters, 2020. **11**(7): p. 2393-2401.

20. Xu, C., et al., *A first-principles investigation of a new hard multi-layered MnB_2 structure.* RSC Advances, 2017. **7**(17): p. 10559-10563.

21. Hu, X.B., et al., *Atomic-scale observation and analysis of chemical ordering in M_3B_2 and M_5B_3 borides.* Acta Materialia, 2018. **149**: p. 274-284.

22. Wang, J., et al., *Discovery of hexagonal ternary phase Ti2InB2 and its evolution to layered boride TiB.* Nature Communications, 2019. **10**(1): p. 2284.

23. Song, Z., et al., *First principles calculation on the newly superhard materials of W-B-C ternary system.* Solid State Communications, 2019. **301**: p. 113705.

24. Kvashnin, A.G., et al., *Computational Search for New W–Mo–B Compounds.* Chemistry of Materials, 2020. **32**(16): p. 7028-7035.

25. Miao, N., et al., *Computational Prediction of Boron-Based MAX Phases and MXene Derivatives.* Chemistry of Materials, 2020. **32**(16): p. 6947-6957.

26. Naumova, A.S., et al., *Unusual Chemistry of the C–H–N–O System under Pressure and Implications for Giant Planets.* The Journal of Physical Chemistry A, 2021. **125**(18): p. 3936-3942.

27. van de Walle, A., *A complete representation of structure–property relationships in crystals.* Nature Materials, 2008. **7**(6): p. 455-458.

28. Magri, R. and A. Zunger, *Real-space description of semiconducting band gaps in substitutional systems.* Phys Rev B Condens Matter, 1991. **44**(16): p. 8672-8684.

29. Ouyang, B., et al., *Cluster Expansion Framework for the $Sr(Ti_{1-x}Fe_x)O_{3-x/2}$ (0 < x < 1) Mixed Ionic Electronic Conductor: Properties Based on Realistic Configurations.* Chemistry of Materials, 2019. **31**(9): p. 3144-3153.

30. Lavrentiev, M.Y., S.L. Dudarev, and D. Nguyen-Manh, *Magnetic cluster expansion simulations of FeCr alloys.* Journal of Nuclear Materials, 2009. **386-388**: p. 22-25.

31. Talapatra, A., et al., *High-throughput combinatorial study of the effect of M site alloying on the solid solution behavior of M_2AlC MAX phases.* Physical Review B, 2016. **94**(10): p. 104106.

32. Arróyave, R. and M. Radovic, *Ab initio investigation of $Ti_2Al(C,N)$ solid solutions.* Physical Review B, 2011. **84**(13): p. 134112.

33. Arróyave, R., et al., *Does aluminum play well with others? Intrinsic Al-A alloying behavior in 211/312 MAX phases.* Materials Research Letters, 2017. **5**(3): p. 170-178.

34. Arróyave, R., et al., *Out-of-plane ordering in quaternary MAX alloys: an alloy theoretic perspective.* Materials Research Letters, 2018. **6**(1): p. 1-12.

35. Wong, Z.M., et al., *High performance photocatalytic and thermoelectric two-dimensional asymmetrically ordered Janus-like MXene alloys.* Materials Advances, 2020. **1**(5): p. 1176-1185.

36. Perdew, J.P., K. Burke, and M. Ernzerhof, *Generalized Gradient Approximation Made Simple.* Physical Review Letters, 1996. **77**(18): p. 3865-3868.

37. Blöchl, P.E., *Projector augmented-wave method.* Physical Review B, 1994. **50**(24): p. 17953-17979.

38. Fredericks, S., et al., *PyXtal: A Python library for crystal structure generation and symmetry analysis.* Computer Physics Communications, 2021. **261**: p. 107810.

39. Dahlqvist, M. and J. Rosen, *Chemical order or disorder – a theoretical stability expose for expanding the compositional space of quaternary metal borides.* Materials Advances, 2022.

40. Saal, J.E., Kirklin, S., Aykol, M., Meredig, B., and Wolverton, C, *Materials Design and Discovery with High-Throughput Density Functional Theory: The Open Quantum Materials Database (OQMD).* JOM, 2013. **65**.

41. Kirklin, S., Saal, J.E., Meredig, B., Thompson, A., Doak, J.W., Aykol, M., Rühl, S. and Wolverton, C, *The Open Quantum Materials Database (OQMD): assessing the accuracy of DFT formation energies.* npj Computational Materials, 2015. **1**.

42. A. Jain*, S.P.O., G. Hautier, W. Chen, W.D. Richards, S. Dacek, S. Cholia, D. Gunter, D. Skinner, G. Ceder, K.A. Persson, *The Materials Project: A materials genome approach to accelerating materials innovation.* APL Materials, 2013. **1**.

43. *Springer Materials: The Landolt-Börnstein database*.

44. Chang, J.H., et al., *CLEASE: A versatile and user-friendly implementation of cluster expansion method.* Journal of Physics Condensed Matter, 2019. **31**(32).

45. Glass, C.W., A.R. Oganov, and N. Hansen, *USPEX—Evolutionary crystal structure prediction.* Computer Physics Communications, 2006. **175**(11): p. 713-720.

46. Ade, M. and H. Hillebrecht, *Ternary Borides Cr_2AlB_2, Cr_3AlB_4, and Cr_4AlB_6: The First Members of the Series $(CrB_2)_nCrAl$ with n = 1, 2, 3 and a Unifying Concept for Ternary Borides as MAB-Phases.* Inorganic Chemistry, 2015. **54**(13): p. 6122-6135.

47. Kota, S., et al., *Synthesis and Characterization of an Alumina Forming Nanolaminated Boride: MoAlB.* Sci Rep, 2016. **6**: p. 26475.

48. Dahlqvist, M., et al., *Origin of Chemically Ordered Atomic Laminates (i-MAX): Expanding the Elemental Space by a Theoretical/Experimental Approach.* ACS Nano, 2018. **12**(8): p. 7761-7770.

Supplementary Files

This is a list of supplementary files associated with this preprint. Click to download.

- SupplementaryInformation.docx